
Centralized and distributed cognitive task processing in the human connectome

Enrico Amico^{1,2}, Alex Arenas³ and Joaquín Goñi^{1,2,4*}

¹ School of Industrial Engineering, Purdue University, West-Lafayette, IN, USA

² Purdue Institute for Integrative Neuroscience, Purdue University, West-Lafayette, IN, USA

³ Departament d'Enginyeria Informàtica i Matemàtiques, Universitat Rovira i Virgili, Tarragona, Spain

⁴ Weldon School of Biomedical Engineering, Purdue University, West-Lafayette, IN, USA

* jgonicor@purdue.edu

Abstract

A key question in modern neuroscience is how cognitive changes in a human brain can be quantified and captured by functional connectomes (FC). A systematic approach to measure pairwise functional distance at different brain states is lacking. This would provide a straight-forward way to quantify differences in cognitive processing across tasks; also, it would help in relating these differences in task-based FCs to the underlying structural network. Here we propose a framework, based on Jensen-Shannon divergence, to map the task-rest connectivity divergence between tasks and resting-state FC. We show how this information theoretical measure allows for quantifying connectivity changes in distributed and centralized processing in functional networks. We study resting-state and seven tasks from the Human Connectome Project dataset to obtain the most divergent links across tasks. We investigate how these changes are associated to different functional brain networks, and use the proposed measure to infer changes in the information processing regimes. Furthermore, we show how the FC divergence with respect to resting state is shaped by structural connectivity, and to what extent this relationship depends on the task. This framework provides a well grounded mathematical quantification of connectivity changes associated to cognitive processing in large-scale brain networks.

Introduction

The progress in neuroimaging methodologies in recent years, together with the rise of publicly available datasets [1, 2] has boosted research on quantitative analysis of brain connectivity patterns based on network science. The intuition of modeling the brain as a network [3–6] has rapidly expanded into the scientific area denominated Brain Connectomics [3, 7]. In brain network models, nodes correspond to grey-matter regions (based on brain atlases or parcellations) while links or edges correspond to structural or functional connections. Structural connections are estimated from diffusion weighted imaging [8, 9] data by modeling white matter pathways through tractography algorithms [10–12]. Functional connections represent statistical dependencies between brain regions time series while subjects are either at rest or performing a task during functional MRI (fMRI) sessions [13]. These functional associations are usually measured via correlations among fMRI time series to study functional connectivity (FC) in the human brain [13, 14].

These recent advances have led the brain connectivity community to start exploring and quantify differences between resting-state FCs and task-based FCs [15–18]. The main lines of research in this direction involved: whole-brain network similarity analyses on the intrinsic and task-evoked network architecture of human connectome [15]; the mapping of cortical hubs and brain region for adaptive task control (so called “cognitive control network” [16, 17]; the investigation of activity flow from resting-state FCs to infer brain regions that carry diverse cognitive task information [17, 19]. Despite all these efforts in trying to characterize connectivity differences between resting-state and task activity in brain networks, a systematic analysis on how to measure pairwise (i.e. at the level of FC links) “cognitive distance” between these different functional states is still lacking. Such a methodology would provide a straight-forward way to quantify differences in cognitive processing across tasks; also, it would help in relating these local differences in task-based FCs to the underlying structural network architecture, another exciting avenue for the brain connectomics community (see our recent work [20]).

Here we propose a framework, based on Jensen-Shannon (JS) divergence [21, 22], to map the “cognitive divergence” between task and resting-state functional connections. We show how this simple measure allows for quantifying the amount of changes in distributed and centralized processing in human functional networks.

We use resting-state and seven different task sessions from the Human Connectome Project (HCP) database to obtain the most JS-divergent edges across tasks. We study how these changes across tasks are associated to different functional brain networks, and use the proposed measure to infer modifications in the information processing regimes of these networks. Furthermore, we show how cognitive divergence is shaped by the brain structural architecture and the level of nestedness of axonal pathways, and to what extent this relationship depends on the task-based functional scenario at hand. We conclude by discussing the new insights offered by this approach, as well as potential applications and future directions.

Methods

Dataset

The fMRI dataset used in this work is from the publicly available Human Connectome Project (HCP, <http://www.humanconnectome.org/>), Release Q3. Per HCP protocol, all subjects gave written informed consent to the Human Connectome Project consortium. Below is the full description of the acquisition protocol and processing steps.

HCP: functional data

We used the 100 unrelated subjects from the HCP 900 subjects data release [1, 2]. The fMRI resting-state runs were acquired in separate sessions on two different days (HCP filenames: rfMRI_REST1 and rfMRI_REST2), with two different acquisitions (left to right or LR and right to left or RL) per day [23, 24]. The seven fMRI tasks were: gambling (tfMRI_GAMBLING), relational (tfMRI_RELATIONAL), social (tfMRI_SOCIAL), working memory (tfMRI_WM), motor (tfMRI_MOTOR), language (tfMRI_LANGUAGE, including both a story-listening and arithmetic task) and emotion (tfMRI_EMOTION). The working memory, gambling and motor task were acquired on the first day, and the other tasks were acquired on the second day [2, 25]. The HCP scanning protocol was approved by the local Institutional Review Board at Washington University in St. Louis. For all sessions, data from both the left-right (LR) and right-left (RL) phase-encoding runs were averaged to calculate connectivity matrices. This operation was done for all 7 fMRI tasks. Full details on the HCP dataset have been published previously [1, 23, 24].

HCP: structural data

We used DWI runs from the same 100 unrelated subjects of the HCP 900 subjects data release [1, 2]. The diffusion acquisition protocol is covered in detail elsewhere [23, 26, 27]. Below we mention the main characteristics. Very high-resolution acquisitions (1.25 mm isotropic) were obtained by using a Stejskal–Tanner (monopolar) [28] diffusion-encoding scheme. Sampling in q-space was performed by including 3 shells at $b = 1000, 2000$ and 3000 s/mm². For each shell corresponding to 90 diffusion gradient directions and 5 $b = 0$ acquired twice were obtained, with the phase encoding direction reversed for each pair (i.e. LR and RL pairs). Directions were optimised within and across shells (i.e. staggered) to maximize angular coverage using the approach of [29] (<http://www.sop.inria.fr/members/Emmanuel.Caruyer/q-space-sampling.php>), and form a total of 270 non-collinear directions for each PE direction. Correction for EPI and eddy current-induced distortions in the diffusion data was based on manipulation of the acquisitions so that a given distortion manifests itself differently in different images [30]. To ensure better correspondence between the phase-encoding reversed pairs, the whole set of diffusion-weighted (DW) volumes is acquired in six separate series. These series were grouped into three pairs, and within each pair the two series contained the same DW directions but with reversed phase-encoding (i.e. a series of M_i DW volumes with RL phase-encoding is followed by a series of M_i volumes with LR phase-encoding, where $i = [1, 2, 3]$).

Brain atlas

We employed a cortical parcellation into 360 brain regions as recently proposed by Glasser et al. [31]. For completeness, 14 sub-cortical regions were added, as provided by the HCP release (filename “Atlas_ROI2.nii.gz”). To do so, this file was converted from NIFTI to CIFTI format by using the HCP workbench software [23, 32] (<http://www.humanconnectome.org/software/connectome-workbench.html>, command `-cifti-create-label`)

HCP preprocessing: functional data

The HCP functional preprocessing pipeline [23, 24] was used for the employed dataset. This pipeline included artifact removal, motion correction and registration to standard space. Full details on the pipeline can be found in [23, 24]. The main steps were: spatial (“minimal”) pre-processing, in both volumetric and grayordinate forms (i.e., where brain locations are stored as surface vertices [24]); weak highpass temporal filtering (> 2000 s full width at half maximum) applied to both forms, achieving slow drift removal. MELODIC ICA [33] applied to volumetric data; artifact components identified using FIX [34]. Artifacts and motion-related time courses were regressed out (i.e. the 6 rigid-body parameter time-series, their backwards-looking temporal derivatives, plus all 12 resulting regressors squared) of both volumetric and grayordinate data [24].

For the resting-state fMRI data, we also added the following steps: global gray matter signal was regressed out of the voxel time courses [35]; a bandpass first-order Butterworth filter in forward and reverse directions [0.001 Hz, 0.08 Hz] [35] was applied (Matlab functions *butter* and *filtfilt*); the voxel time courses were z-scored and then averaged per brain region, excluding outlier time points outside of 3 standard deviation from the mean, using the workbench software (workbench command `-cifti-parcellate`). For task fMRI data, we applied the same above mentioned steps but we opted for a more liberal bandpass filter [0.001 Hz, 0.25 Hz], since it is still unclear the connection between different tasks and optimal frequency ranges [15].

Pearson correlation coefficients between pairs of nodal time courses were calculated (MATLAB command *corr*), resulting in a symmetric connectivity matrix for each fMRI

session of each subject. As aforementioned, data from both the left-right (LR) and right-left (RL) phase-encoding runs were averaged to calculate individual functional connectomes in each fMRI session. Functional connectivity matrices were kept in its signed weighted form, hence neither thresholded nor binarized. Finally, the resulting individual functional connectivity matrices were ordered (rows and columns) according to 7 functional cortical sub-networks (FNs) as proposed by Yeo and colleagues [36]. For completeness, an 8th sub-network including the 14 HCP sub-cortical regions was added (as analogously done in recent papers [20, 37]).

HCP preprocessing: structural data

The HCP DWI data were processed following the MRtrix3 [9] guidelines (http://mrtrix.readthedocs.io/en/latest/tutorials/hcp_connectome.html). In summary, we first generated a tissue-segmented image appropriate for anatomically constrained tractography (ACT [11], MRtrix command `5ttgen`); we then estimated the multi-shell multi-tissue response function ([38], MRtrix command `dwi2response msmt_5tt`) and performed the multi-shell, multi-tissue constrained spherical deconvolution ([39], MRtrix `dwi2fod msmt_csd`); afterwards, we generated the initial tractogram (MRtrix command `tckgen`, 10 million streamlines, maximum tract length = 250, FA cutoff = 0.06) and applied the successor of Spherical-deconvolution Informed Filtering of Tractograms (SIFT2, [12]) methodology (MRtrix command `tcksift2`). Both SIFT [40] and SIFT2 [12] methods provides more biologically meaningful estimates of structural connection density. SIFT2 allows for a more logically direct and computationally efficient solution to the streamlines connectivity quantification problem: by determining an appropriate cross-sectional area multiplier for each streamline rather than removing streamlines altogether, biologically accurate measures of fiber connectivity are obtained whilst making use of the complete streamlines reconstruction [12]. Finally, we mapped the SIFT2 outputted streamlines onto the 374 chosen brain regions (360 from Glasser et al. [31] brain atlas plus 14 subcortical regions, see Brain Atlas section) to produce a structural connectome (MRtrix command `tck2connectome`). Finally, a \log_{10} transformation [3] was applied on the structural connectomes to better account for differences at different magnitudes. In consequence, SC values ranged between 0 and 5 on this dataset.

Jensen-Shannon divergence on functional edges

The Jensen-Shannon divergence is a method commonly used to measure dissimilarities between two probability distributions [21, 22, 41]. In the case of two discrete probability distributions P and Q , the Jensen-Shannon divergence (JSD) is defined by:

$$JSD(P||Q) = \frac{1}{2}D_{KL}(P||M) + \frac{1}{2}D_{KL}(Q||M) \quad (1)$$

where $M = \frac{1}{2}(P + Q)$ and D_{KL} is the Kullback-Leibler divergence [22]. For two discrete probability distributions P and Q , it is defined by:

$$D_{KL}(P||Q) = - \sum_i P(i) \log \frac{Q(i)}{P(i)} \quad (2)$$

For the particular case of measuring the dissimilarity between two probability distributions P and Q , the Jensen-Shannon divergence is bounded between 0 and 1, given that one uses the base 2 logarithm:

$$0 \leq JSD(P||Q) \leq 1 \quad (3)$$

We used the *JSD* to map “connectivity divergence” between resting state and task sessions. Here we assume resting state to be the “cognitive baseline”, and we measured the *JSD* distance link to link from every task FCs to resting state FCs. Below follows a detailed description of the procedure (see also scheme at Fig. 1). First, for every edge in a functional connectome, we extract the corresponding individual values (as many as subjects in the cohort, i.e. 100 in this paper). In this study, this resulted in having two vectors with 100 elements, one for each resting state edge and one for each edge in the task FCs whose JS distance is to be evaluated. These vectors represent Pearson’s correlation distributions of connectivity values across all subjects in the cohort. Secondly, we transform these two Pearson’s distributions into discrete probability distributions. We sampled the $[-1, 1]$ Pearson’s range via uniform binning (bin width = 0.2), and counted the likelihood of occurrence of the connectivity values in each bin. Finally, the *JSD* between these two probability distributions was computed for every edge and HCP task considered in this study. This edgewise functional connectivity distance from resting-state can be seen as task-specific connectivity divergence. That is, how far is the distribution of values in a specific task with respect to the resting-state FC baseline.

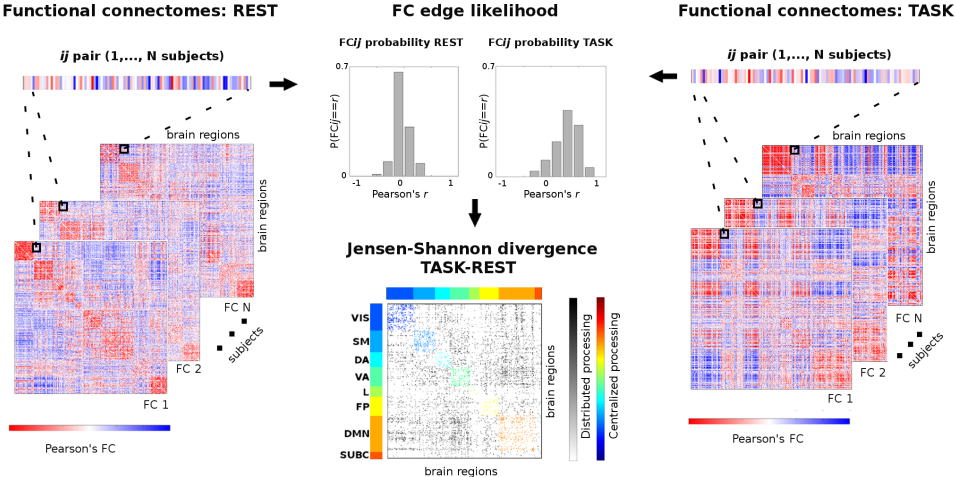


Figure 1. Workflow scheme for task-rest connectivity divergence. This scheme summarizes the procedure to measure edgewise distance from a cohort of N functional connectomes (FCs) at rest (left) to a task-based one (right). First, an edge ij is extracted from the set, for both the resting-state and task-based FCs; these two vectors of N connectivity values are then transformed into probability distributions (center top); finally, the Jensen-Shannon divergence [21] for these two edgewise probabilities is computed (center bottom). Iterating this procedure over all possible ij pairs gives a Jensen-Shannon (JS) matrix of local divergence in task FCs with respect to the REST baseline. The JS matrix is ordered by the 7 functional networks (FNs): visual (VIS), somato-motor (SM), dorsal attention (DA), ventral attention (VA), limbic (L), frontoparietal (FP), default mode network (DMN). An eighth subcortical network (SUBC) is added for completeness. Within-networks most distant edges are color-coded according FNs. Between-networks most divergent edges are in grayscale. This methods allows for quantifying the changes between centralized (within-network) and distributed (between-network) processing when a specific task is performed with respect to the resting-state baseline.

Centralized and distributed processing in functional connectomes

The aforementioned procedure produced 374×374 (i.e. number of regions in the employed brain atlas) JSD matrices per each task. Next, we sought to relate the proposed connectivity divergence measure with changes in functional processing across functional networks (FNs). To do so, we first thresholded the JSD matrices based on the 95th percentile of the entire JSD distribution of values across all tasks, to select only the most distant links from resting-state (see Fig. 2). Next, we quantify the amount of change in each of the 8 functional FNs (see HCP preprocessing: functional data section for details on the chosen FNs) by counting the number of edges that survived the threshold divided by the total number of edges present in each FN. We can then formalize changes in centralized processing (CP), for each functional network k , as:

$$CP^k = \frac{\sum_{i,j \in WN^k} \widehat{JSD}_{ij}}{\sum_{i,j \in WN^k} WN_{ij}^k} \quad (4)$$

Where \widehat{JSD} is the binary version of the JSD matrix thresholded at 95 percentile (1 for surviving edges, 0 elsewhere) for a specific task, and WN^k is a binary matrix of the same size as \widehat{JSD} , with 1 if an edge falls within functional network k , and 0 elsewhere. Similarly, one can quantify changes in distributed processing (DP) as:

$$DP^{kl} = \frac{\sum_{i,j \in BN^{kl}} \widehat{JSD}_{ij}}{\sum_{i,j \in BN^{kl}} BN_{ij}^{kl}} \quad (5)$$

Where now BN^{kl} is a binary matrix of the same size as \widehat{JSD} , with 1 if an edge falls between functional networks k, l , and 0 elsewhere.

Hence, for each one of the 8 functional networks considered here (see HCP preprocessing: functional data for details), one can obtain one value of CP and 7 values of DP (considering all pairwise FNs interactions), for a specific task. These values provide an estimate of the density of the most connectivity divergent functional links across within and between FN connectivity. That is, the amount of local changes in distributed and centralized processing in each FN from baseline, defined as resting-state functional connectivity.

Surrogate null model evaluation for connectivity divergence analysis

To validate the JSD results in functional connectomes, we tested the same approach on randomized counterparts (or “surrogates”) of the original data. To do so, we employed the Amplitude Adjusted Fourier Transform (AAFT) surrogates method [42] to obtain data random surrogates. Starting from the 374 fMRI time series (one per brain region in the atlas, see also Brain atlas) we generated AAFT fMRI time series surrogates as proposed in [42]. This method aims to build surrogate time series that preserve the amplitude distribution and the power spectrum of the original data [42].

For each of the seven HCP tasks and resting-state, we computed 100 surrogate versions of the functional connectivity matrices, and then evaluated number of non-zero elements in $\widehat{JSD}_{\text{surrogate}}$ for each of the 100 realizations. This provided null distributions (one per task) for the connectivity divergence measure, that allowed us to test whether or not the results obtained on the original FCs were statistically significant.

Estimation of functional connectivity divergence associations with structural connectomes

Next, we sought to assess the role of structural connections in the connectivity divergence of functional links across all seven tasks. In order to do so, we divided the group-averaged structural connectivity (SC) weights (see HCP preprocessing: structural data for details on SC computation) into 5 different percentile intervals $\{0 - 20; 20 - 40; 40 - 60; 60 - 80; 80 - 100\}$. We then counted the average number of most divergent edges (i.e. the non-zero elements of \widehat{JSD}) falling in each of the 5 percentile intervals, for each of the seven HCP task. This provides an estimate on the relationship between structural connections and connectivity divergence and whether it depends on the specific task being performed. We also tested whether centralized and distributed processing depend on the “nestedness” or “hiddenness” of the structural pathways, as measured by search information [43–45]. Search information quantifies the accessibility or hiddenness of the shortest path between a source node and a target node within the network by measuring the amount of knowledge or information in bits needed to access the path [43–46]. The more nested the shortest path between two brain regions ij , the higher its SI value; conversely, the less hidden or integrated the path, the lower its the SI value. Similarly to the experiment performed on SC weights, we again divided the group-average SI range of values into 5 different percentile intervals: $\{0 - 20; 20 - 40; 40 - 60; 60 - 80; 80 - 100\}$. Finally, we counted the average number of most divergent edges (i.e. the non-zero elements of \widehat{JSD}) falling in each of the 5 SI percentile intervals, for each of the seven HCP task. This provides an estimate on the relationship between structural “hiddenness” and connectivity divergence and its associations with the specific task being performed. For both SC weights and SI, the significance of the associations with centralized and distributed processing was assessed through one-way analysis of variance (ANOVA [47], Matlab command *anova1*), with “observations” being centralized and distributed processing values for the 7 tasks, and “groups” being the 5 percentile intervals described above.

Results

The dataset used for this study consisted of functional data from the 100 unrelated subjects in the Q3 release of the HCP [1, 2]. We defined the “connectivity divergence” between task FC links and resting-state FC links as the edgewise Jensen Shannon divergence (JSD) between resting-state FCs and task FCs (see also scheme at Fig. 1). This distance metric quantify the connectivity divergence of a functional link recruited in a task with respect to its correspondent “usage” in resting-state. For each of the 7 HCP tasks (see Methods for details), we computed the correspondent JSD matrix, and extracted the most connectivity divergent edges (≥ 95 percentile distribution of JSD values across all tasks; Fig. 2, see also Jensen-Shannon divergence on functional edges for details on the methodology).

Notably, the results obtained are significantly different from the same analyses performed on 100 realizations of surrogate data built from the fMRI time series considered in this study (Fig. 5 and Table ??, see Surrogate null model evaluation for connectivity divergence analysis for details). This confirms that the results that follow are not arising by chance neither due to the thresholding procedure employed.

Interestingly, the level of divergence from resting state seems to be associated to the specific task (Fig. 2). For some task, the within-functional network links are more divergent, i.e. more involved (e.g., for the Emotion and Motor tasks), in other the between-FNs connections are the most divergent ones (i.e., Relational or Working memory tasks). The dichotomy between intra-network (i.e. centralized) and inter-

MOST JS-DISTANT FUNCTIONAL EDGES (>95 prctile) FROM REST

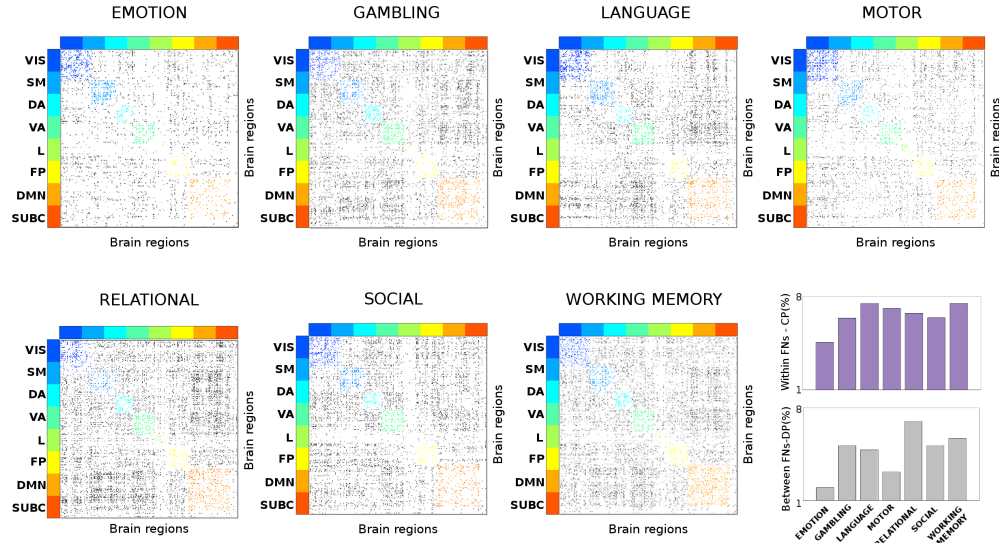


Figure 2. Connectivity divergence across different tasks. Evaluation of the most divergent functional links (in terms of Jensen-Shannon (JS) distance, see Methods) across 7 different task sessions. The JS matrices were thresholded at the 95% of the distribution of JS values across the seven tasks. The JS matrices then ordered by 7 functional networks (FNs, [36]): visual (VIS), somato-motor (SM), dorsal attention (DA), ventral attention (VA), limbic (L), frontoparietal (FP), default mode network (DMN). An eight subcortical network (SUBC) was added for completeness. The edges surviving the threshold corresponding to within-FN connections color-coded accordingly. Edges corresponding to between-FN connections are depicted in grayscale. Note how the connectivity divergence depends on the task: in some cases within-FNs connectivity are more recruited (i.e., for the Emotion task), in other between-FNs connections are the most divergent (i.e., Relational task). The bottom-right bar plots depict the average percentage of within-FNs most divergent edges, i.e. centralized processing (CP, violet bars) and the average percentage of between-FNs edges, i.e. distributed processing (DP, grey bars) across the different tasks.

network (i.e. distributed) divergence led us to quantify the changes in centralized and distributed processing in task FCs (Fig. 3, see also the Centralized and distributed processing in functional connectomes section).

Note how, for two functional networks, i.e. frontoparietal and default mode, there is a clear demarcation between centralized and distributed processing, for all the seven tasks evaluated (Fig. 3). This indicates that the two networks increase the amount of distributional processing more when they are recruited in a task than in resting-state. Furthermore, with the exception of limbic and subcortical networks, where little difference in centralized and distributed processing can be observed (Fig. 3), in all the other FNs (i.e., visual, somato-motor, dorsal and ventral attention) there is balance between intra and inter-network processing. This trade-off seems to depend on the task at hand (slightly more centralized in some, more distributed in others, Fig. 3).

In order to determine whether changes in task processing are related to the underlying structural connectivity, we first evaluated the relationship between connectivity divergence in each task and structural connectivity weights (Fig. 4, A1-B1). Interestingly, a significant trend arises for all task between centralized processing and number of tracts

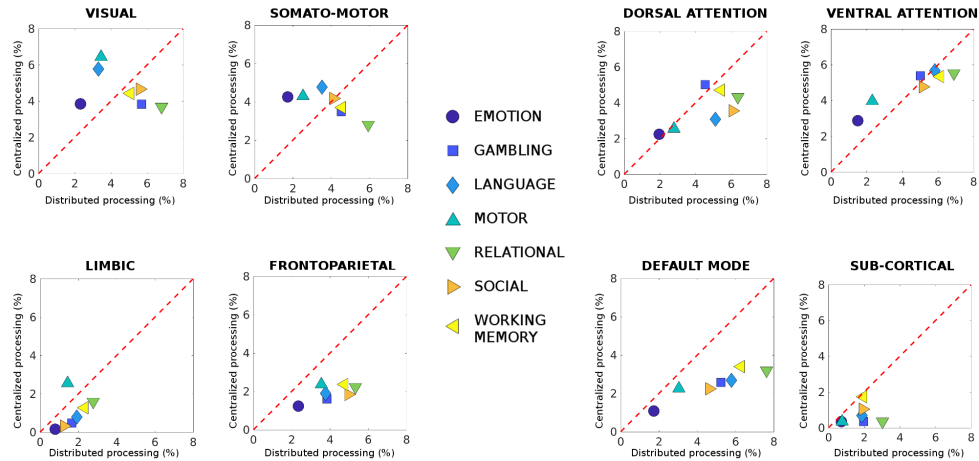


Figure 3. Centralized and distributed task processing in functional connectomes. Each plot shows differences in centralized versus distributed processing (see Methods) for each of the seven functional networks (FNs, visual, somato-motor, dorsal and ventral attention, limbic, frontoparietal, DMN, [36]) and sub-cortical network, for all the seven different HCP tasks. The difference in centralized processing with respect to resting state was defined as the number of most Jensen-Shannon (JS) divergent edges within-FN divided by the total number of edges in the FN (reported as percentage). Similarly, deviations from distributed processing in resting-state were defined as the number of most JS-divergent edges between FN divided by the total number of between FN connections. Note how FP and DMN networks deviate from rest mainly in the amount of distributed processing, i.e. between-FNs connectivity.

(one-way ANOVA $p < 0.01$, Fig. 4, A1). That is, the more structurally connected two regions are within a functional network, the higher the increase in centralized processing when recruited in a task. Notice how this trend is general and independent from the task, albeit the magnitude of this linear association between structure and cognitive depends on the task at hand (Fig. 4, A1). On the other hand, when looking at changes in distributed processing, i.e. for edges involved in between-functional network connectivity, no significant associations with structural connectivity were observed (Fig. 4, B1).

We then dug deeper into the relationship between task processing and structural connectome by evaluating the level of hiddenness or accessibility of a structural path, as measured by search information [43] (see also Estimation of functional connectivity divergence associations with structural connectomes for details), and testing its association with changes in cognitive task processing (Fig. 4A2-B2). Interestingly, the hiddenness of structural paths appears to be inversely related to changes in centralized processing (one-way ANOVA $p < 0.01$, Fig. 4, A2). That is, the more “isolated” the structural pathway between two brain regions within a functional network, the higher will be its recruitment in a task. The more nested or integrated the path, the less divergent the centralized processing with respect to resting state (Fig. 4, A2). No significant associations were found when looking at changes in distributed processing versus search information range of values (Fig. 4, B2).

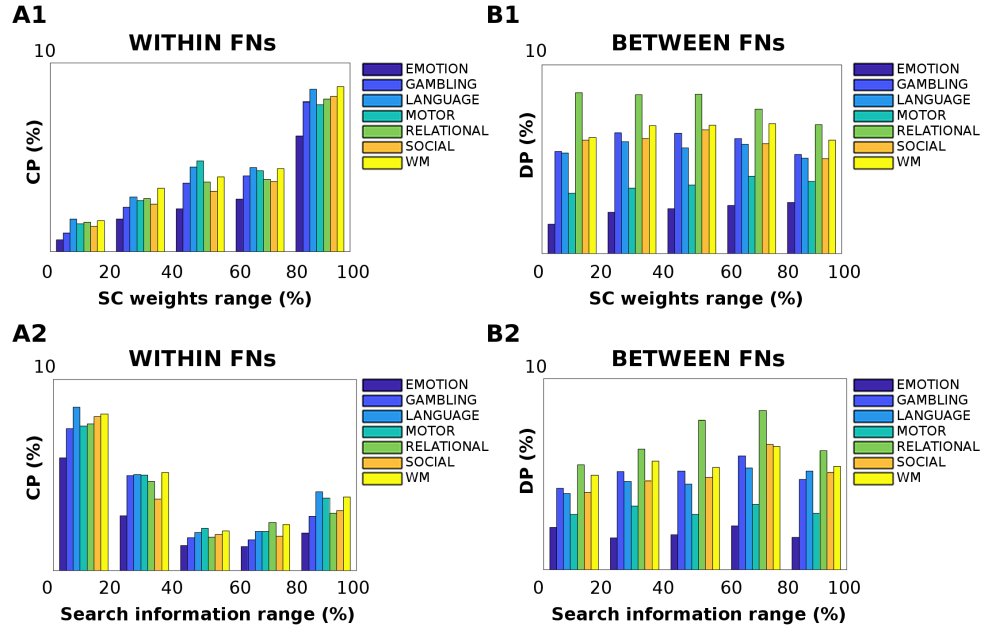


Figure 4. Effect of structural pathways on centralized and distributed processing changes. A1-B1) The dependence of structural connections on the average Jensen-Shannon distance was evaluated across the seven different tasks. The bar plots shows the percentage of increase in centralized processing (CP) within functional networks (FNs, A1) and distributed processing (DP) between FNs (B1), per 5 different percentile range of structural connectivity weights: 0 – 20, 20 – 40, 40 – 60, 60 – 80 and 80 – 100. The percentile range was extracted from the group-averaged structural connectome. Note how, for within-FNs connections (A1), the increase in centralized processing significantly correlates with the strength of structural connections across all tasks (one-way ANOVA $p < 0.01$); conversely, the underlying structural connectivity does not play a major role in distributed processing changes. **A2-B2)** The effect of structural path accessibility (as measured by search information, see Methods) on centralized and distributed processing was tested across the seven different tasks, per 5 different percentile intervals of search information: 0-20, 20-40, 40-60, 60-80 and 80-100. The percentile range was extracted from the group-averaged search information matrix. Notably, increase in centralized processing (A2) are significantly associated to low values of SI (one-way ANOVA $p < 0.01$); conversely, the nestedness of the structural pathways does not play a significant role in distributed processing changes.

Discussion

Cognitive brain network mapping [16, 17], or the analysis of brain network features underlying task performance and cognitive control [15, 48], is a recent and exciting new line of investigation in brain connectomics. While the general intrinsic common architecture between resting state and task-based functional patterns has been explored [15], still very little is known about task connectivity divergences and their associations to information processing [16, 19]. Furthermore, an even more intricate question relates to the relationship between the different task-based FC scenarios and the underlying structural connectivity [20].

Here we addressed these questions by proposing a novel methodology in neuroscience, rooted to the concept of Jensen-Shannon divergence [21, 41], to measure task-based

pairwise functional distance with respect to the “cognitive baseline” defined by resting-state FCs (Fig. 1). This framework may also be seen from a multilayer perspective, with the ground layer being resting-state FCs and top layers defined by the multiple task-based different connectivity scenarios. The distance defined here can be thought as inter-layer coupling, or as the amount of cognitive processing necessary to make the “cognitive switch” from the resting-state ground layer to the top task-based functional layers.

The work presented here complements the aforementioned recent studies on cognitive mapping, where the resting state scaffolding was usually used to infer or also predict task changes in connectivity [15, 19, 48]. Here we evaluate and investigate the pairwise distance task-rest, and use it to map specific changes dictated by the task at hand. This adds up to previous studies in that it improves our understanding of how edge specific is the cognitive switch, and its level of recruitment (in terms of “connectivity divergence”), as well as in terms of centralized and distributed processing changes in functional networks (Fig. 2).

We exploited this new concept of connectivity divergence to infer about the level of recruitment of an edge or of a functional network (Fig. 2). Notably, the connectivity divergent patterns present in the original data were significantly different from the ones obtained by surrogate data built from the original fMRI time series (Fig. 5 and Table ??). Indeed, the more divergent a functional network in a specific task, the more different its recruitment with respect to resting-state. Hence, the more changes in cognitive information processing that functional subsystem will undergo. This intuition led us to explore the concept of centralized and distributed processing in large scale functional networks, that we defined as the difference between intra (i.e. centralized)-and inter (i.e. distributed) network connectivity (Fig. 3). Interestingly, two functional networks (frontoparietal and DMN) showed major changes in distributed processing and very minor changes in centralized processing, for all the seven tasks evaluated with respect to resting state (Fig. 3). This is in line with recent findings showing that frontoparietal areas appear to be the more flexible for cognitive control and task performance [16, 17].

The fact that this network and the DMN, which is well-known to play a major role in resting-state [49–51], change mainly in terms of inter-communication when transitioning to task, is also noteworthy. This finding goes along with the concept of integration of information between neural subsystems [52] and also with our recent findings on the association between FP-DMN dis-connectivity and degradation in arousal and levels of consciousness [37]. Possibly, the more demanding the task, the more the cross-talk between FP, DMN and rest of the brain network might be needed to achieve the proper amount of cognitive processing.

Another major question relates to how these changes in cognitive processing are shaped or determined by the underlying structural architecture of a human brain. Very few studies so far have tried to elucidate the relationship between cognitive changes and axonal pathways, either for localized cortical subsystems (e.g. fusiform gyrus [53]) or a specific task (e.g. visual stimuli [54]). In a recent work we tackled this problem from in a whole-brain network fashion, by means of ICA-based approach to extract the main “hybrid” functional-structural connectivity features sensitive to cognitive changes across seven different tasks [20].

Here we took this investigation one step further by assessing functional connectivity divergence associations with respect to the underlying structural connectivity weights (Fig. 4). Interestingly, for changes in centralized processing, the relationship with structural connectivity is linear (Fig. 4A1). That is, when the cognitive processing involves mainly within-network connectivity, the higher the fiber strength between two regions, the more divergent they will be. Nonetheless, this relationship is not present when looking at distributed processing link to link effects (Fig. 4B1). This might imply

that the between network connectivity links can play a key role in the creation of more complex cognitive regimes. The cross-talk between functional networks might bring the brain network up to a more integrated level, allowing for a more dynamic and distributed cognitive processing, that ultimately deviates far from the static underlying boundaries given by the structural fiber tracts.

To test this hypothesis, we evaluated the relationship between changes in distributed and centralized processing and structural path “hiddenness” or accessibility, as measured by search information ([43], see also Estimation of functional connectivity divergence associations with structural connectomes). Notably, when looking at centralized processing deviations from rest, these two quantities appear to be inversely related (Fig. 4A2,B2). The less integrated the path between two regions within a functional network, the higher the value in centralized processing, the more integrated the structural pathways, the less centralized activity (Fig. 4A2).

These findings corroborate the hypothesis on the integration segregation in the human brain [52]. It is also in line with our findings on the importance of cross-talking between functional networks for task changes ([20]), which can be summarized as follows: for a human brain to make a cognitive switch, a delicate interplay between centralized and distributed processing is necessary. The centralized activity within functional subsystems is shaped by brain structure. Moreover, the more isolated the shortest path connecting two centralized brain regions, the higher the level of task processing (Fig. 4). However, in order to achieve proper cognitive complexity for the task at hand, an appropriate level of distributed processing and subsequent integration between these subsystems is needed: the level of cross-talking and structural integration will depend on the specific task at hand (Fig. 2, Fig. 4) and on the functional subnetwork involved (Fig. 3), with no significant function-structure associations (Fig. 4).

This study has several limitations. The effect of different brain atlases (here we used the one proposed by Glasser et al. [31]) and functional network organization (here we used the one proposed by Yeo et al. [36]) on the centralized and processing changes should be explored. Because of the way it is defined, the measure does not allow for individualized connectivity divergence patterns. However, future studies could explore to what extent individual FCs can be predicted by group-wise changes in centralized and distributed processing, or use the information on the most divergent link at the group level to select the most meaningful pairwise connectivity for the task at hand. Finally, the simplicity of the methodology allows for its applicability in the clinical domain, where it could be employed to measure connectivity divergence between “healthy” and “diseased” populations (e.g. Alzheimer, schizophrenia, coma etc.), or to determine task-rest divergence in situations where the cognitive switch is damaged or disrupted (e.g. in autism or similar neurological disorders).

In conclusion, we have reported a new methodology that aims at capturing the functional differences between different tasks when compared to resting state. The methodology based on the Jensen-Shannon divergence is promising, and has been proved to discern between centralized and distributed activity across brain areas for different tasks. These results pave the way to the usage of this framework in other experiments, and to the development of a new information-theoretical framework for the analysis of functional and structural connectomes.

Acknowledgments

Data were provided [in part] by the Human Connectome Project, WU-Minn Consortium (Principal Investigators: David Van Essen and Kamil Ugurbil; 1U54MH091657) funded by the 16 NIH Institutes and Centers that support the NIH Blueprint for Neuroscience Research; and by the McDonnell Center for Systems Neuroscience at Washington

University. This work was partially supported by NIH R01EB022574 and by NIH R01MH108467 and by the Indiana Clinical and Translational Sciences Institute (Grant Number UL1TR001108) from the National Institutes of Health, National Center for Advancing Translational Sciences, Clinical and Translational Sciences Award. AA acknowledges financial support from Spanish MINECO (grant FIS2015-71582-C2-1), Generalitat de Catalunya ICREA Academia, and the James S. McDonnell Foundation.

Author Contributions

E.A, A.A. and J.G conceptualized the study, designed the framework, interpreted the results and wrote the manuscript. E.A. and J.G. processed the MRI data and performed the analyses.

References

1. D. C. Van Essen, K. Ugurbil, E. Auerbach, D. Barch, T. E. J. Behrens, R. Bucholz, A. Chang, L. Chen, M. Corbetta, S. W. Curtiss, S. Della Penna, D. Feinberg, M. F. Glasser, N. Harel, A. C. Heath, L. Larson-Prior, D. Marcus, G. Michalareas, S. Moeller, R. Oostenveld, S. E. Petersen, F. Prior, B. L. Schlaggar, S. M. Smith, A. Z. Snyder, J. Xu, E. Yacoub, and WU-Minn HCP Consortium, “The Human Connectome Project: a data acquisition perspective,” *NeuroImage*, vol. 62, pp. 2222–2231, Oct. 2012.
2. D. C. Van Essen, S. M. Smith, D. M. Barch, T. E. J. Behrens, E. Yacoub, and K. Ugurbil, “The WU-Minn Human Connectome Project: An overview,” *NeuroImage*, vol. 80, pp. 62–79, Oct. 2013.
3. A. Fornito, A. Zalesky, and E. Bullmore, *Fundamentals of Brain Network Analysis*. Academic Press, Mar. 2016.
4. O. Sporns, “The human connectome: a complex network,” *Annals of the New York Academy of Sciences*, vol. 1224, pp. 109–125, Apr. 2011.
5. E. Bullmore and O. Sporns, “Complex brain networks: graph theoretical analysis of structural and functional systems,” *Nature Reviews Neuroscience*, vol. 10, pp. 186–198, Mar. 2009.
6. D. S. S. Bassett and E. Bullmore, “Small-world brain networks.,” *The Neuroscientist : a review journal bringing neurobiology, neurology and psychiatry*, vol. 12, pp. 512–523, Dec. 2006.
7. A. Fornito, A. Zalesky, and M. Breakspear, “The connectomics of brain disorders,” *Nature Reviews Neuroscience*, vol. 16, pp. 159–172, Mar. 2015.
8. D. L. Bihan, “Looking into the functional architecture of the brain with diffusion MRI,” *Nature Reviews Neuroscience*, vol. 4, p. 469, June 2003.
9. J.-D. Tournier, S. Mori, and A. Leemans, “Diffusion tensor imaging and beyond,” *Magnetic Resonance in Medicine*, vol. 65, pp. 1532–1556, June 2011.
10. J.-D. Tournier, F. Calamante, and A. Connelly, “MRtrix: Diffusion tractography in crossing fiber regions,” *International Journal of Imaging Systems and Technology*, vol. 22, pp. 53–66, Mar. 2012.

11. R. E. Smith, J.-D. Tournier, F. Calamante, and A. Connelly, "Anatomically-constrained tractography: Improved diffusion MRI streamlines tractography through effective use of anatomical information," *NeuroImage*, vol. 62, pp. 1924–1938, Sept. 2012.
12. R. E. Smith, J.-D. Tournier, F. Calamante, and A. Connelly, "SIFT2: Enabling dense quantitative assessment of brain white matter connectivity using streamlines tractography," *NeuroImage*, vol. 119, pp. 338–351, Oct. 2015.
13. M. P. van den Heuvel and H. E. Hulshoff Pol, "Exploring the brain network: A review on resting-state fMRI functional connectivity," *European Neuropsychopharmacology*, vol. 20, pp. 519–534, Aug. 2010.
14. M. D. Fox and M. E. Raichle, "Spontaneous fluctuations in brain activity observed with functional magnetic resonance imaging," *Nature Reviews Neuroscience*, vol. 8, pp. 700–711, Sept. 2007.
15. M. W. Cole, D. S. Bassett, J. D. Power, T. S. Braver, and S. E. Petersen, "Intrinsic and Task-Evoked Network Architectures of the Human Brain," *Neuron*, vol. 83, pp. 238–251, July 2014.
16. M. W. Cole and W. Schneider, "The cognitive control network: Integrated cortical regions with dissociable functions," *NeuroImage*, vol. 37, pp. 343–360, Aug. 2007.
17. M. W. Cole, J. R. Reynolds, J. D. Power, G. Repovs, A. Anticevic, and T. S. Braver, "Multi-task connectivity reveals flexible hubs for adaptive task control," *Nature Neuroscience*, vol. 16, p. 1348, Sept. 2013.
18. J. Gonzalez-Castillo, Z. S. Saad, D. A. Handwerker, S. J. Inati, N. Brenowitz, and P. A. Bandettini, "Whole-brain, time-locked activation with simple tasks revealed using massive averaging and model-free analysis," *Proceedings of the National Academy of Sciences*, vol. 109, no. 14, pp. 5487–5492, 2012.
19. T. Ito, K. R. Kulkarni, D. H. Schultz, R. D. Mill, R. H. Chen, L. I. Solomyak, and M. W. Cole, "Cognitive task information is transferred between brain regions via resting-state network topology," *Nature Communications*, vol. 8, p. 1027, Oct. 2017.
20. E. Amico and J. Goñi, "Mapping hybrid functional-structural connectivity traits in the human connectome," *arXiv:1710.02199 [q-bio]*, Oct. 2017. arXiv: 1710.02199.
21. J. Briët and P. Harremoës, "Properties of classical and quantum Jensen-Shannon divergence," *Physical Review A*, vol. 79, p. 052311, May 2009.
22. T. M. Cover and J. A. Thomas, *Elements of Information Theory*. John Wiley & Sons, Nov. 2012. Google-Books-ID: VWq5GG6ycxMC.
23. M. F. Glasser, S. N. Sotiropoulos, J. A. Wilson, T. S. Coalson, B. Fischl, J. L. Andersson, J. Xu, S. Jbabdi, M. Webster, J. R. Polimeni, D. C. Van Essen, and M. Jenkinson, "The minimal preprocessing pipelines for the Human Connectome Project," *NeuroImage*, vol. 80, pp. 105–124, Oct. 2013.
24. S. M. Smith, C. F. Beckmann, J. Andersson, E. J. Auerbach, J. Bijsterbosch, G. Douaud, E. Duff, D. A. Feinberg, L. Griffanti, M. P. Harms, M. Kelly, T. Laumann, K. L. Miller, S. Moeller, S. Petersen, J. Power, G. Salimi-Khorshidi, A. Z. Snyder, A. T. Vu, M. W. Woolrich, J. Xu, E. Yacoub, K. Uğurbil, D. C. Van Essen, and M. F. Glasser, "Resting-state fMRI in the Human Connectome Project," *NeuroImage*, vol. 80, pp. 144–168, Oct. 2013.

-
25. D. M. Barch, G. C. Burgess, M. P. Harms, S. E. Petersen, B. L. Schlaggar, M. Corbetta, M. F. Glasser, S. Curtiss, S. Dixit, C. Feldt, D. Nolan, E. Bryant, T. Hartley, O. Footer, J. M. Bjork, R. Poldrack, S. Smith, H. Johansen-Berg, A. Z. Snyder, and D. C. Van Essen, "Function in the human connectome: Task-fMRI and individual differences in behavior," *NeuroImage*, vol. 80, pp. 169–189, Oct. 2013.
 26. S. N. Sotiropoulos, S. Jbabdi, J. Xu, J. L. Andersson, S. Moeller, E. J. Auerbach, M. F. Glasser, M. Hernandez, G. Sapiro, M. Jenkinson, D. A. Feinberg, E. Yacoub, C. Lenglet, D. C. Van Essen, K. Ugurbil, and T. E. J. Behrens, "Advances in diffusion MRI acquisition and processing in the Human Connectome Project," *NeuroImage*, vol. 80, pp. 125–143, Oct. 2013.
 27. K. Ugurbil, J. Xu, E. J. Auerbach, S. Moeller, A. T. Vu, J. M. Duarte-Carvajalino, C. Lenglet, X. Wu, S. Schmitter, P. F. Van de Moortele, J. Strupp, G. Sapiro, F. De Martino, D. Wang, N. Harel, M. Garwood, L. Chen, D. A. Feinberg, S. M. Smith, K. L. Miller, S. N. Sotiropoulos, S. Jbabdi, J. L. R. Andersson, T. E. J. Behrens, M. F. Glasser, D. C. Van Essen, and E. Yacoub, "Pushing spatial and temporal resolution for functional and diffusion MRI in the Human Connectome Project," *NeuroImage*, vol. 80, pp. 80–104, Oct. 2013.
 28. E. O. Stejskal and J. E. Tanner, "Spin Diffusion Measurements: Spin Echoes in the Presence of a Time-Dependent Field Gradient," *The Journal of Chemical Physics*, vol. 42, pp. 288–292, Jan. 1965.
 29. E. Caruyer, J. Cheng, C. Lenglet, G. Sapiro, T. Jiang, and R. Deriche, "Optimal Design of Multiple Q-shells experiments for Diffusion MRI," Sept. 2011.
 30. J. L. R. Andersson, S. Skare, and J. Ashburner, "How to correct susceptibility distortions in spin-echo echo-planar images: application to diffusion tensor imaging," *NeuroImage*, vol. 20, pp. 870–888, Oct. 2003.
 31. M. F. Glasser, T. S. Coalson, E. C. Robinson, C. D. Hacker, J. Harwell, E. Yacoub, K. Ugurbil, J. Andersson, C. F. Beckmann, M. Jenkinson, S. M. Smith, and D. C. Van Essen, "A multi-modal parcellation of human cerebral cortex," *Nature*, vol. 536, pp. 171–178, Aug. 2016.
 32. D. Marcus, J. Harwell, T. Olsen, M. Hodge, M. Glasser, F. Prior, M. Jenkinson, T. Laumann, S. Curtiss, and D. Van Essen, "Informatics and Data Mining Tools and Strategies for the Human Connectome Project," *Frontiers in Neuroinformatics*, vol. 5, 2011.
 33. M. Jenkinson, C. F. Beckmann, T. E. J. Behrens, M. W. Woolrich, and S. M. Smith, "FSL," *NeuroImage*, vol. 62, pp. 782–790, Aug. 2012.
 34. G. Salimi-Khorshidi, G. Douaud, C. F. Beckmann, M. F. Glasser, L. Griffanti, and S. M. Smith, "Automatic denoising of functional MRI data: Combining independent component analysis and hierarchical fusion of classifiers," *NeuroImage*, vol. 90, pp. 449–468, Apr. 2014.
 35. J. D. Power, A. Mitra, T. O. Laumann, A. Z. Snyder, B. L. Schlaggar, and S. E. Petersen, "Methods to detect, characterize, and remove motion artifact in resting state fMRI," *NeuroImage*, vol. 84, pp. 320–341, Jan. 2014.
 36. B. T. T. Yeo, F. M. Krienen, J. Sepulcre, M. R. Sabuncu, D. Lashkari, M. Hollinshead, J. L. Roffman, J. W. Smoller, L. Zöllei, J. R. Polimeni, B. Fischl,

-
- H. Liu, and R. L. Buckner, "The organization of the human cerebral cortex estimated by intrinsic functional connectivity," *Journal of Neurophysiology*, vol. 106, pp. 1125–1165, Sept. 2011.
37. E. Amico, D. Marinazzo, C. Di Perri, L. Heine, J. Annen, C. Martial, M. Dzemidzic, M. Kirsch, V. Bonhomme, S. Laureys, and J. Goñi, "Mapping the functional connectome traits of levels of consciousness," *NeuroImage*, vol. 148, pp. 201–211, Mar. 2017.
38. D. Christiaens, M. Reisert, T. Dhollander, S. Sunaert, P. Suetens, and F. Maes, "Global tractography of multi-shell diffusion-weighted imaging data using a multi-tissue model," *NeuroImage*, vol. 123, pp. 89–101, Dec. 2015.
39. B. Jeurissen, J.-D. Tournier, T. Dhollander, A. Connelly, and J. Sijbers, "Multi-tissue constrained spherical deconvolution for improved analysis of multi-shell diffusion MRI data," *NeuroImage*, vol. 103, pp. 411–426, Dec. 2014.
40. R. E. Smith, J.-D. Tournier, F. Calamante, and A. Connelly, "SIFT: Spherical-deconvolution informed filtering of tractograms," *NeuroImage*, vol. 67, pp. 298–312, Feb. 2013.
41. M. D. De Domenico, V. Nicosia, A. Arenas, and V. Latora, "Structural reducibility of multilayer networks," *Nature Communications*, vol. 6, p. 6864, Apr. 2015.
42. T. Schreiber and A. Schmitz, "Surrogate time series," *Physica D: Nonlinear Phenomena*, vol. 142, pp. 346–382, Aug. 2000.
43. J. Goñi, M. P. v. d. Heuvel, A. Avena-Koenigsberger, N. V. d. Mendizabal, R. F. Betzel, A. Griffa, P. Hagmann, B. Corominas-Murtra, J.-P. Thiran, and O. Sporns, "Resting-brain functional connectivity predicted by analytic measures of network communication," *Proceedings of the National Academy of Sciences*, vol. 111, pp. 833–838, Jan. 2014.
44. A. Trusina, M. Rosvall, and K. Sneppen, "Communication boundaries in networks," *Physical review letters*, vol. 94, no. 23, p. 238701, 2005.
45. M. Rosvall, A. Grönlund, P. Minnhagen, and K. Sneppen, "Searchability of networks," *Physical Review E*, vol. 72, no. 4, p. 046117, 2005.
46. J. Wirsich, A. Perry, B. Ridley, T. Proix, M. Golos, C. Bénar, J.-P. Ranjeva, F. Bartolomei, M. Breakspear, V. Jirsa, *et al.*, "Whole-brain analytic measures of network communication reveal increased structure-function correlation in right temporal lobe epilepsy," *NeuroImage: Clinical*, vol. 11, pp. 707–718, 2016.
47. R. V. Hogg and J. Ledolter, *Engineering statistics*. Macmillan Pub Co, 1987.
48. I. Tavor, O. P. Jones, R. B. Mars, S. M. Smith, T. E. Behrens, and S. Jbabdi, "Task-free MRI predicts individual differences in brain activity during task performance," *Science*, vol. 352, pp. 216–220, Apr. 2016.
49. M. E. Raichle, "The Brain's Default Mode Network," *Annual Review of Neuroscience*, vol. 38, no. 1, pp. 433–447, 2015.
50. M. E. Raichle, A. M. MacLeod, A. Z. Snyder, W. J. Powers, D. A. Gusnard, and G. L. Shulman, "A default mode of brain function," *Proceedings of the National Academy of Sciences*, vol. 98, pp. 676–682, Jan. 2001.

-
51. M. D. Greicius, B. Krasnow, A. L. Reiss, and V. Menon, "Functional connectivity in the resting brain: A network analysis of the default mode hypothesis," *Proceedings of the National Academy of Sciences*, vol. 100, pp. 253–258, Jan. 2003.
 52. G. Tononi, O. Sporns, and G. M. Edelman, "A measure for brain complexity: relating functional segregation and integration in the nervous system," *Proceedings of the National Academy of Sciences*, vol. 91, pp. 5033–5037, May 1994.
 53. Z. M. Saygin, D. E. Osher, K. Koldewyn, G. Reynolds, J. D. Gabrieli, and R. R. Saxe, "Anatomical connectivity patterns predict face selectivity in the fusiform gyrus," *Nature neuroscience*, vol. 15, no. 2, pp. 321–327, 2012.
 54. D. E. Osher, R. R. Saxe, K. Koldewyn, J. D. Gabrieli, N. Kanwisher, and Z. M. Saygin, "Structural connectivity fingerprints predict cortical selectivity for multiple visual categories across cortex," *Cerebral Cortex*, vol. 26, no. 4, pp. 1668–1683, 2015.

Supportive Information

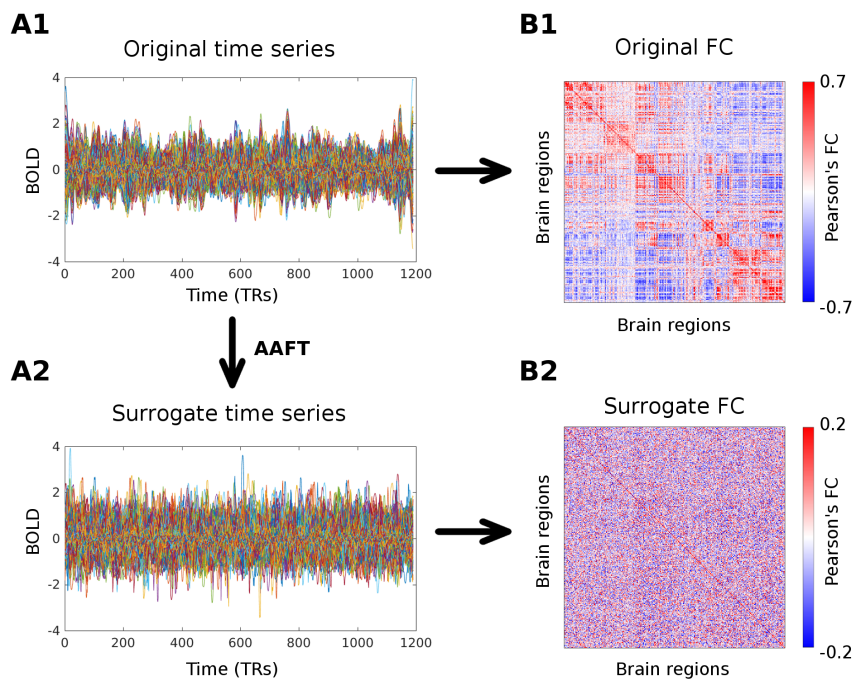


Figure 5. Scheme of the functional connectome randomization procedure. In order to validate the JSD results in functional connectomes (FC), we used “surrogates” of the original data. We here show an example of this procedure for one subject, resting-state. The original BOLD 374 (i.e. one per brain region) time series (A1), from which the FC was originated (B1), were randomized by means of the Amplitude Adjusted Fourier Transform (AAFT) surrogates method ([42], see Surrogate null model evaluation for connectivity divergence analysis for details). These randomized time-series (A2) were then used for the construction of the surrogate FC of the subject (B2).

Task name	Most divergent edges median+99% Surrogate	Most divergent edges Original values
Emotion	132 ± 36	1655
Gambling	18 ± 14	3736
Language	8 ± 9	3648
Motor	4 ± 7	2625
Relational	40 ± 19	4856
Social	376 ± 46	3732
Working Memory	1 ± 3	4161

Table 1. Null models for cognitive divergence. Table reports, for each task, the median (and $\pm 99\%$ confidence intervals of the distribution) values for the most divergent edges obtained from 100 realization of FC surrogates. The surrogates were built from the original fMRI time series using the Amplitude Adjusted Fourier Transform randomization procedure ([42], see Surrogate null model evaluation for connectivity divergence analysis for details. Note how the original values of most divergent edges are always significantly different from the surrogate null distribution (i.e. above the 99 percentile), for all the seven HCP tasks considered in this study.